JOURNAL OF PROPULSION AND POWER
Vol. 27, No. 3, May–June 2011

Mechanism of Propagation Direction of Rotating Cavitations in a Cascade

Yuka Iga*
Tohoku University, Sendai 980-8577, Japan
and
Yoshiki Yoshida†
Japan Aerospace Exploration Agency, Kakuda 981-1525, Japan

DOI: 10.2514/1.49454

The propagation mechanism of rotating cavitations, especially that of supersynchronous rotating cavitation, is still unclear. The direction of propagation of supersynchronous rotating cavitation is in the direction of rotation of an impeller, which is opposite of the direction of rotating stall in general pumps and fans. Also, neither the mechanism of the order of appearance of rotating cavitations (supersynchronous, synchronous, and subsynchronous propagation) nor the mechanism of the discontinuity of the propagation speed during the transition between different types of rotating cavitations has been determined thus far. The present study indicates that they can be explained by the existence of latent rotating stall and a specific feature of cavitation: a decrease in the break-off frequency of a cavitation according to its development.

Nomenclature

C	=	chord length
C_L	=	lift coefficient
C_p	=	pressure coefficient
$\mathbf{E}$	=	flux vector
$\mathbf{Ev}$	=	viscous vector
f	=	frequency
h	=	pitch
K_l	=	liquid constant
PVR	=	propagation velocity ratio
p	=	static pressure
p_c	=	pressure constant of gas phase
p_v	=	saturated vapor pressure
Q	=	mass flow rate
$\mathbf{Q}$	=	unknown variable vector
R_g	=	gas constant
$\mathbf{S}$	=	source-term vector
T	=	temperature
T_c	=	temperature constant of gas phase
U	=	velocity
u	=	velocity component
Y	=	mass fraction of gas phase
α	=	void fraction (volume fraction of gas phase)
α_{in}	=	inflow angle
Γ	=	evaporation speed
γ	=	stagger angle
μ	=	viscosity
ρ	=	density
σ	=	cavitation number
τ	=	stress tensor
ϕ	=	flow rate coefficient
ψ	=	static pressure coefficient

Subscripts

a	=	axial
cav	=	cavitation
g	=	gas phase
in	=	inlet boundary
l	=	liquid phase
out	=	outlet boundary
t	=	tangential
th	=	cascade throat entrance

I. Introduction

UNSTEADY cavitation in an inducer, which is an axial-flow pump installed at the inlet of a turbopump in a liquid-propellant rocket engine, sometimes leads to the unstable oscillation of the turbopump. This phenomenon, known as cavitation instability, can be classified into two kinds of instabilities: 1) rotating cavitation accompanied by asynchronous and synchronous axial vibration and 2) cavitation surge accompanied by pulsation of the working fluid. The occurrence mechanism of cavitation surge, which results from system instability, has been largely clarified in many previous studies. On the other hand, the occurrence mechanism of rotating cavitation, which results from local instability, has not yet been completely explained. That is, it is still unclear why supersynchronous rotating cavitation propagates in the direction opposite the usual rotating stall observed in pumps and fans. It is known that the occurrence of rotating cavitation is characterized by regularity: with decreasing pressure under the condition of a constant flow rate, supersynchronous, then synchronous, followed by subsynchronous rotating cavitation occur in actual three- and four-blade inducers [1,2]. The reverse order has not been observed in the past, although sometimes only one type of rotating cavitation occurs. A similar order has also been reproduced in numerical simulation of a four-blade cascade [3]. In addition, it is known that there is no continuity during the transition from one type of rotating cavitation to another; that is, the propagation speed is discontinuous. For example, in a three-blade inducer, the propagation speeds are 1.1 to 1.25 (supersynchronous), 1.0 (synchronous), and 0.8 to 0.9 (subsynchronous) times the rotating speed of the inducer [1].

Meanwhile, in the field of numerical simulation of cavitation, many numerical methods and models have been developed. At an early stage, several methods and models were proposed: a one-fluid method in which only the liquid phase outside the cavity is calculated

Received 18 February 2010; revision received 12 November 2010; accepted for publication 19 November 2010.

*Institute of Fluid Science, Katahira 2-1-1, Aoba-ku, Miyagi.
†Kakuda Space Center, Koganezawa 1, Kimigaya, Miyagi.

[4], a bubble flow model in which the behavior of bubbles that constitute the cavity are tracked [5], and a one-fluid two-phase method in which gas and liquid phases inside and outside the cavity are treated as a continuum, such as a barotropic model based on barotropic equation of state [6] or using a pseudodensity equation [7]. By using numerical methods, two-dimensional steady and unsteady flowfields around a hydrofoil were calculated. In recent years, sufficiently developed numerical methods or computational codes have been proposed: UNCLE-M [8], which takes into account the noncondensable gas [9] in the cavity and uses the preconditioning method to calculate low-Mach-number flowfields by a compressible scheme; the full cavitation model [10], which solves the reduced Rayleigh–Plesset equation by taking into account the turbulence effect in phase-change (probability density function model [11]) and noncondensable gas; and CRUNCH CFD [12], which can be applied to simulation of a three-dimensional complex flowfield by extension to an unstructured grid system and can be applied to a cryogenic flowfield by taking into account the thermodynamic effect of cavitation.

Also, the present authors have developed a numerical method based on a compressible homogeneous model that is suitable for calculation of unsteady cavitation [13]. In addition, we have reproduced the frequency characteristics of the break-off phenomenon of sheet cavitation and have clarified two mechanisms of the break-off phenomenon in the cascade [14]. We have also reproduced two types of cavitation instabilities: rotating cavitations and cavitation surge, which occur by different mechanisms, through numerical analysis of the three-blade cyclic cascade, without adding a model or boundary condition for individual phenomena [15]. In the cited study, the occurrence condition or the propagation velocity ratio, which have been well documented based on experimental results, were reproduced qualitatively. Additionally, the possibility of the suppression of cavitation instabilities by a jet flow through a slit on cascade blades was reported [16] and the mass flow gain factor and cavitation compliance were numerically estimated and the occurrence region of cavitation instabilities and frequency of cavitation surge were examined by using the dynamic parameter of cavitation [17]. Additionally, by coupling the Lagrangian calculation of few bubbles in the cavitating flowfield to the above Eulerian calculation in which cavitating flowfield is treated homogeneously, a method of predicting the erosion intensity distribution around a hydrofoil has been developed [18]. Therefore, the numerical method developed by present authors was confirmed to be applicable for numerical simulation of cavitation instabilities that occur due to mutual interference between the oscillation of unsteady cavitation and the fluid machinery.

In a previous study [15], we proposed a mechanism for the propagation direction of supersynchronous rotating cavitation: namely, the superposition of two rotating-stall cells. However, the waveform of the throat flow rate observed in the present study cannot be explained by the previously proposed mechanism, and thus we propose another mechanism that can explain the three types of rotating cavitation by a unified rule. By reproducing various kinds of cavitation instabilities through numerical simulation of a three-blade cyclic cascade and by analyzing the unsteady characteristics of sheet cavitation in the instabilities, we consider a mechanism for the propagation direction, the appearance order, and the discontinuity of the propagation speed during the transition of rotating cavitations.

II. Numerical Method for Cavitating Flow

A. Locally Homogeneous Model of Compressible Gas–Liquid Two-Phase Medium

In this study, a locally homogeneous model of compressible gas–liquid two-phase medium [14] is used for the numerical simulation of cavitation. In this model, by considering the gas–liquid two-phase field as a pseudo single-phase medium, Navier–Stokes (N-S) equations for continuum can be applied to a cavitating flowfield in which there is discontinuity between the gas and liquid phases. The governing equations for the gas–liquid medium are the following compressible gas–liquid N-S equations [14]:

$$\frac{\partial \mathbf{Q}}{\partial t}+\frac{\partial(\mathbf{E}_j-\mathbf{Ev_j})}{\partial x}=\mathbf{S},\qquad \mathbf{Q}=\begin{pmatrix}\rho\\ \rho u_i\\ \rho Y\end{pmatrix}$$

$$\mathbf{E}_j=\begin{pmatrix}\rho u_j\\ \rho u_i u_j+\delta_{ij}p\\ \rho u_j Y\end{pmatrix},\qquad \mathbf{Ev}_\mathrm{j}=\begin{pmatrix}0\\ \tau_{ij}\\ 0\end{pmatrix},\qquad \mathbf{S}=\begin{pmatrix}0\\ 0\\ \Gamma\end{pmatrix} \tag{1}$$

where ρ, p, and u are the density, static pressure, and velocity of the mixture phase, respectively, and Y is the mass fraction of the gas phase. Viscosity of the mixture phase μ, needed to estimate stress tensor τ in Eq. (1), is estimated as follows:

$$\mu=(1-\alpha)(1+2.5\alpha)\mu_l+\alpha\mu_g \tag{2}$$

where α is the volume fraction of the gas phase (void fraction), and subscripts g and l denote gas and liquid phases, respectively.

The governing equations in Eq. (1) are closed by an equation of state for the locally homogeneous compressible gas–liquid two-phase medium [14]. The equation of state is derived as follows by a local equilibrium assumption of pressure and temperature between the gas and liquid phases and a linear combination of the mass of the liquid phase with that of the gas phase, where the liquid phase allows compressibility and the gas phase is considered to be an ideal gas:

$$\rho=\frac{p(p+p_c)}{K_l(1-Y)p(T+T_c)+R_gY(p+p_c)T} \tag{3}$$

where K_l is the liquid constant, R_g is the gas constant, and p_c and T_c are the pressure and temperature constants of the liquid, respectively.

The speed of sound of the two-phase medium derived from Eq. (3) was verified, and found to be in good agreement with the experimental value concerning variation of the void fraction [14]. Therefore, this numerical method can be used to reproduce pressure-wave propagation in a mixed flowfield of gas–liquid phases, which is important for the numerical simulation of mutual interference between cavitation and a fluid machinery system.

$\mathbf{S}$ is the source term and Γ is the evaporation speed that expresses evaporation under the condition of instantaneous equilibrium. Γcorresponds to the modification of p and Y, as described below, using the predictors ρ^*, Y^*, and p^*, which are obtained by calculating Eq. (1) with $\mathbf{S}=0$:

$$\begin{aligned}&\rho^{n+1}=\rho^*,\qquad p^{n+1}=\delta p^*+(1-\delta)p_v,\\ &Y^{n+1}=\delta Y^*+(1-\delta)(Y^*+\Delta Y)\\ &=\delta Y^*+(1-\delta)\frac{p_v(p_v-p_c)-\rho^*K_lp_v(T+T_c)}{\rho^*R_g(p_v+p_c)T-\rho^*K_lp_v(T+T_c)},\\ &\delta=\begin{cases}1 & (p^*\geq p_v)\\ 0 & (p^*<p_v)\end{cases}\end{aligned} \tag{4}$$

where p_v is the saturated vapor pressure. Since empirical constants for phase-change speed are not necessary in the above instantaneous-equilibrium evaporation model, it is robust for pressure-wave propagation with a rapid pressure jump. Therefore, the model can be applied with no distinction to flowfields with and without cavitation surge or other phenomena.

Since the cavity surface (i.e., the discontinuity of density) is described as a gradient of the void fraction, the numerical method of the contact discontinuity problem in a compressible fluid can be applied. Consequently, the cavity form is not restricted, although the thickness of the cavity surface depends on the resolution of computational grids. Therefore, this numerical method can be used in the numerical analysis of a wide range of cavitation conditions, except for incipient cavitation.

B. Numerical Scheme

In this study, the governing equations given in Eq. (1) are solved using the finite difference method. Because it is necessary to stably

simulate discontinuities of a large density jump at the gas–liquid interface in a cavitating flowfield, the total-variation-diminishing (TVD) scheme, which ensures the monotonicity of the solution, is used. Specifically, the explicit TVD–MacCormack scheme [19] with second-order accuracy in time and space is used. The order of the time interval in calculation is 10^{-8} in the present study.

C. Validation of the Numerical Method

The present numerical method has been validated for the time-averaged lift and drag of a hydrofoil under cavitation and non-cavitation conditions and time-averaged pressure distribution on a cascade blade under noncavitation conditions with several angles of attack [14]. In the present study, the availability for the unsteady characteristics of sheet cavitation was validated because a target of this study is rotating cavitation. Before that, mesh convergence was examined for the pressure distribution on a NACA0015 hydrofoil [20] under noncavitation conditions (Fig. 1, top) and cavitation conditions (Fig. 1, bottom). The mesh points are set at 100 points around the hydrofoil in rough mesh, 300 points in moderate mesh, and 500 points in fine mesh. Results are shown with results of Reynolds-averaged Navier–Stokes (RANS) calculation (Baldwin–Lomax model with Degani–Schiff modification) for comparison. In the calculations of both noncavitating and cavitating flowfields, the time-averaged pressure distribution on the suction side roughly converges in moderate mesh. Therefore, a mesh system of 300 mesh points around each blade of the cascade is also used in the present study. In the noncavitation condition (Fig. 1, top), excessive reduction of pressure is seen in the last half of the suction side, accompanied by artificial separation, and underestimation of 40% is seen in the suction peak in the calculation without the turbulence model. On the other hand, those factors are suppressed in the calculation with the RANS model, and pressure distribution is roughly predicted, although the suction peak is still somewhat underestimated. The reason underestimating suction peak is that the present calculation was performed in external flow and the imposed blockage effect seems to be slightly insufficient. Under the condition of cavitation (Fig. 1, bottom), both calculations with and without the turbulence model show excessive reduction of pressure in the last half of the suction side in the moderate- and fine-mesh systems. This means that the present RANS model for single-phase flow is not applicable to a pressure distribution on hydrofoil in an unsteady cavitating flowfield. Additionally, although the maximum sheet cavity length is more than the chord length in the experiment, it is about 90% chord length in the calculation using the moderate- and fine-mesh systems with the RANS model. On the other hand, it is close to chord length in the calculation without the turbulence model. This means that the calculation without the present RANS model tends to be applicable to the prediction of aspect of sheet cavity.

Next, using the moderate-mesh system, unsteady sheet cavitation is calculated on the same hydrofoil, and the break-off frequency of sheet cavitation caused by a reentrant jet is estimated for several cavitation numbers, as shown in Fig. 2 such frequency being expressed by Strouhal number based on chord length. For purposes of comparison, experimental values of the peak frequency of pressure fluctuation on the suction side of the hydrofoil are shown in the same figure, which includes noncavitation condition. Under the conditions of cavitation inception, which is around $\sigma = 1.4$ in the present calculation, the resulting break-off frequency shown by calculation without the turbulence model has a much higher value than the experimental frequency. This is because the calculation without the turbulence model fails to reproduce the pressure distribution on the suction side under noncavitation conditions, as shown in Fig. 1. On the other hand, under conditions of fully developed cavitation that is $\sigma < 1.25$, the resulting break-off frequency from the calculation without the turbulence model can better predict the experimental characteristics of frequency compared with that by RANS calculation. In this condition, the frequency by the RANS calculation takes slightly higher values than those calculated without the turbulence model because the RANS calculation tends to slightly underestimate the sheet cavity length, as mentioned above.

Therefore, it is shown that the present RANS model is applicable for calculation of a noncavitating flowfield, but it does not contribute to calculation of unsteady cavitation, which is the intended flowfield of the present study. In the literature, it has often been reported that excess viscosity around termination of a sheet cavity prevents the unsteadiness of the cavity when a RANS model for single-phase flow is used. So, a modified method in which the excess viscosity is decreased in a two-phase condition was developed [21], and it is applied to renormalization group k-ε [21–23], shear stress transport k-ω [24], and Spalart–Allmaras [25]. Although the unsteady behavior of cavitation can be improved so that it is numerically

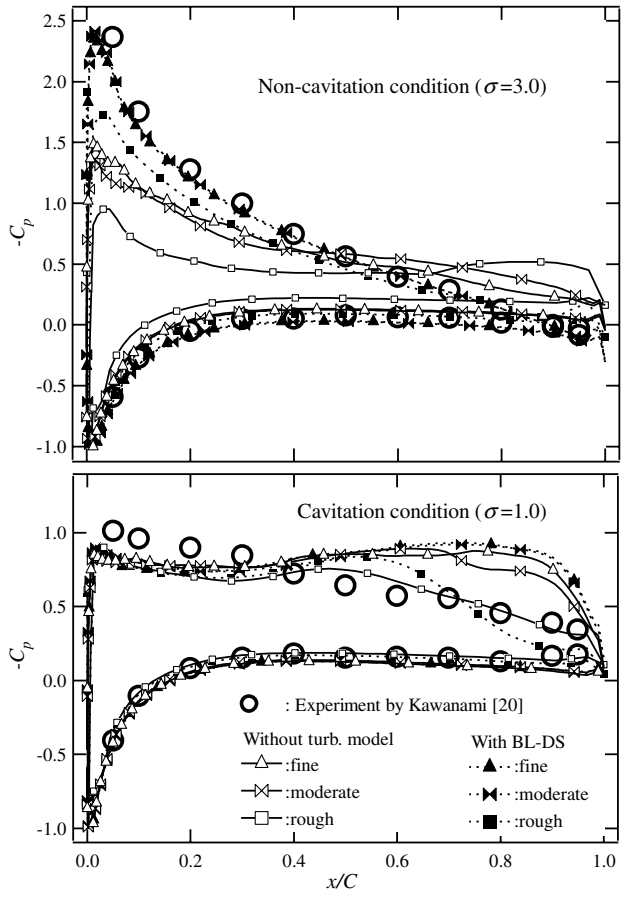

Fig. 1 Mesh convergence of the present numerical method for noncavitating and cavitating flowfield around NACA0015 hydrofoil ($\alpha_{in} = 8$ deg., $U_{in} = 8$ m/s, and $Re = 1.3 \times 10^6$).

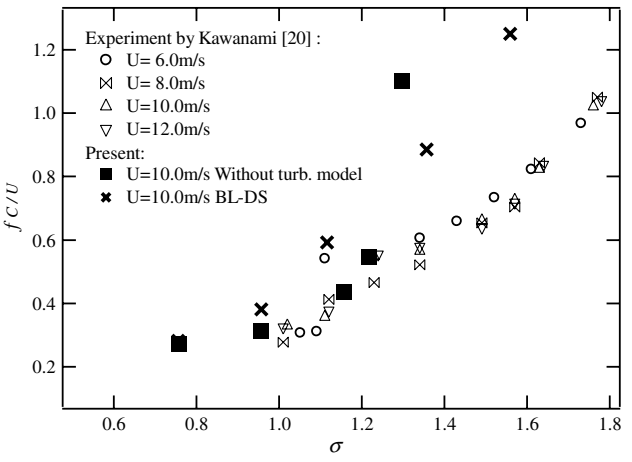

Fig. 2 Validation of break-off frequency of sheet cavitation in an NACA0015 hydrofoil ($\alpha_{in} = 8.36$ deg).

reproducible, no time-averaged lift and drag or time-averaged pressure distribution on a hydrofoil or break-off frequency of sheet cavity agrees with that in the experiment. Thus it can be said that the problem still remains in the turbulence model for calculation of cavitation. Consequently, no turbulence model was applied in the present study because no reliable turbulence model for studying the characteristics of oscillation in cavitation instabilities exists and in order to reduce computational load. However, macroscopic disturbance in the flowfield that is yielded by oscillation of cavity volume is resolved by the present numerical method without use of the turbulence model.

D. Computational Condition

The target flowfield is a three-blade cyclic flat-plate cascade, as shown in Fig. 3, in which solidity is $C/h = 2.0$, the stagger angle is $\gamma = 75°$, blade chord length is $C = 0.1$ m, and thickness is zero. The cascade arrangement is referred to in a previous report on a theoretical study [26]. Calculations were performed not only for a cascade where the three blades had equal lengths, but also for a cascade where the leading edge of one blade was slightly cut so that synchronous rotating cavitation could easily occur.

One cascade passage has 261×71 mesh points and measures two chord lengths from the inlet boundary to the leading edge of the blade and three chord lengths from the trailing edge to the outlet boundary. At the inlet boundary, constant conditions of flow angle, void fraction, and total pressure are applied; static pressure is extrapolated, and velocity is calculated from the condition of constant total pressure. At the outlet boundary, a constant static pressure condition is applied, and velocity and density are extrapolated. The mesh near the inlet and outlet boundaries is sufficiently coarse in order to suppress an artificial reflection of pressure wave from the boundaries. Also, the constant total pressure condition at the inlet boundary can suppress the artificial reflection because both pressure and velocity can change there. A nonslip condition is assumed at the wall boundary of the blades. In addition, a cyclic boundary condition is imposed at every three cascade passages in order to reproduce circumferential instabilities in a cascade, such as rotating cavitation. Hereafter, the blades are denoted as blade 1, blade 2, and blade 3 in the direction opposite the rotation of the cascade, assuming cascade rotation, as shown in Fig. 3.

The inflow angle is selected for a wide range: $\alpha_{\text{in}} = 3$ to 11°. Inflow velocity is about $U_{\text{in}} = 12$ m/s. Computation is performed for several cases of cavitation number σ at each inlet inflow angle, where σ is controlled by changing the outlet static pressure while maintaining a constant flow velocity. Cavitation number σ, flow rate coefficient ϕ, static pressure coefficient ψ, and the propagation velocity ratio (PVR) of rotating cavitation are estimated as follows:

Cavitation number:

$$\sigma = \frac{p_{\text{in}} - p_v}{\frac{1}{2}\rho_{\text{in}} U_{\text{in}}^2} \tag{5}$$

Flow rate coefficient:

$$\phi = U_a / U_t \tag{6}$$

Static pressure constant:

$$\psi = \frac{p_{\text{out}} - p_{\text{in}}}{\rho_{\text{in}} U_t^2} \tag{7}$$

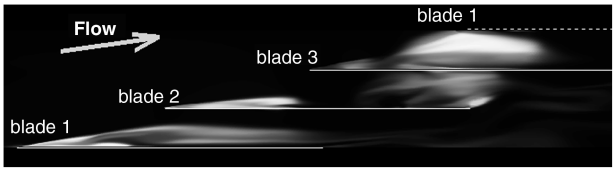

Fig. 3 Aspect of cavitation in the present three-blade cyclic flat-plate cascade ($C/h = 2.0$, $\gamma = 75°$).

Propagation velocity ratio:

$$\text{PVR} = \frac{U_t + U_{\text{cav}}}{U_t} \tag{8}$$

where subscript in means in the inlet boundary; U_t and U_a are the circumferential and axial velocities of U_{in}; U_{cav} is the velocity of the apparent circumferential propagation of the uneven cavity area; and σ and ψ are calculated from the time-averaged computational results of each case. Flow angles $\alpha_{\text{in}} = 3, 5, 7, 9, 9.5$, and 11° correspond to $\phi = 0.213, 0.176, 0.141, 0.105, 0.0963$, and 0.0699, respectively.

III. Results and Discussion

A. Prediction of Occurrence of Rotating Cavitations

The variation in the head performance of the present cascade results is shown in Fig. 4, with a changing cavitation number σ at each angle of attack. The figure is also colored according to predicted cavitation instabilities. The occurrence of cavitation instabilities is judged by the visualization of aspects of the cavity and waveforms of variations in cavity volume and upstream pressure. In the present study, four types of rotating phenomena were detected:

1) A supersynchronous rotating cavitation (super-S RC) is when the uneven cavity volume seems to propagate in the rotational direction of the cascade (blade 3–blade 2–blade 1).

2) A subsynchronous rotating cavitation (sub-S RC) is when the uneven cavity volume seems to propagate in the direction opposite to that of cascade rotation (blade 1–blade 2–blade 3).

3) A synchronous rotating cavitation (sync RC) is when the uneven cavity volume remains attached to each blade.

4) A rotating-stall cavitation (R-stall C) is distinguished from sub-S RC, even though the uneven cavity volume seems to propagate in a direction opposite to that of rotation, because the oscillating characteristic is different from that of sub-S RC. The difference between sub-S RC and R-stall C will be described later.

Furthermore, the differences between the three types of cavitation surge (CS type 1, type 2, and type 3) will be reported elsewhere.

The regions where each rotating phenomenon occurs can be seen to be scattered in Fig. 4, but they follow a certain rule when they are ordered according to flow rate and cavitation number, as shown in Fig. 5. Super-S RC occurs at all flow rates, which corresponds to angles of attack ranging from 3, to 11°. Sub-S RC occurs at a middle flow rate of 7 to 9°, and R-stall C occurs at a lower flow rate of 9.5 to 11°. Sync RC is observed only in the calculation of the cascade where a leading edge is cut into a blade (uneven blade cascade), which is performed at 3°. Furthermore, the occurrence order of the occurrence of rotating phenomena can be seen in Fig. 5 to follow a decrease in cavitation number: sync RC, sub-S RC, and R-stall C occur after super-S RC, although only two rotating phenomena occur at each flow rate. The order of appearance of rotating phenomena observed

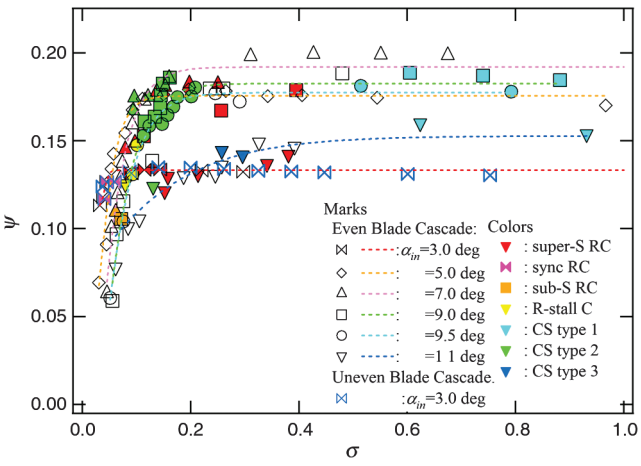

Fig. 4 Head performance of the present cascade and occurrence of cavitation instabilities.

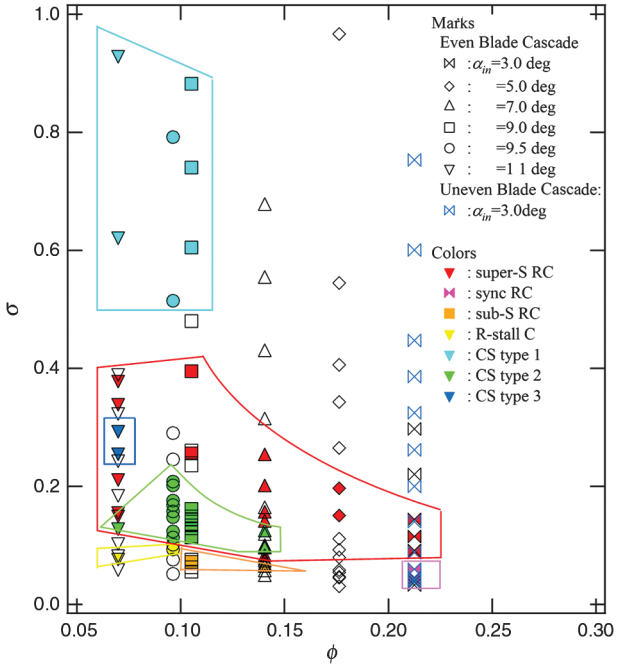

Fig. 5 Occurrence map of cavitation instabilities of the present three-blade cyclic cascade.

in the present study is consistent with the well-known order of rotating cavitations in an actual inducer with three and four blades [1,2], except for R-stall C.

B. Propagation Speeds of Rotating Cavitations

The apparent velocities of the circumferential propagation of an uneven cavity volume in rotating cavitations are calculated from the present numerical results. These velocities are converted to a PVR, which is shown in Fig. 6 and includes all flow rates. The PVR is 1.2 to 1.45 in super-S RC, 1.0 in sync RC, and 0.75 in sub-S RC in the present cascade arrangement. In an actual three-blade inducer, propagation speeds of rotating cavitations have been observed to be 1.1 to 1.25, 1.0, and 0.87 times the rotating speed of the inducer, respectively [1]. Therefore, the present result shows similar propagation characteristics of rotating cavitations, even though there is a difference in the geometric features between the sheet cavitation in the present two-dimensional cascade and the tip vortex cavitation in the actual three-dimensional inducer.

On the other hand, the PVR of R-stall C, at 0.45, is about 60% that of sub-S RC. At this time, the propagation velocity of the uneven cavity volume in R-stall C is over 2 times that of sub-S RC, which means that the cavities in each rotating phenomenon have quite

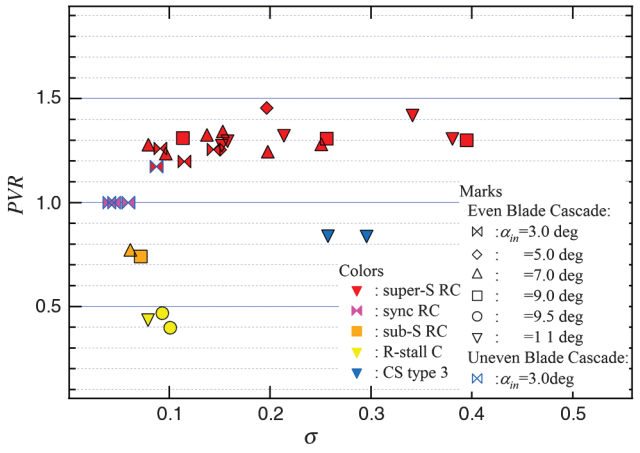

Fig. 6 Propagation velocity ratio of uneven cavity volume in each rotating phenomenon.

different unsteady characteristics. In an actual three-blade inducer, a similar propagation speed of the rotating-stall-type phenomenon with cavitation has been observed in actual three- and two-blade inducers [27,28].

C. Relation Between Lift and Flow Rate Variations

Typical waveforms of the lift variations of each of the three blades (Fig. 7, top) and flow rates in each of the three throats (Fig. 7, bottom) are shown for each rotating phenomenon. The lifts change with the break-off cycle of unsteady sheet cavitations in each blade. For example, the time when the lift of blade 2 is at its maximum value and the lift of blade 1 is at its minimum corresponds with the time when the cloud cavity released from the sheet cavity on blade 1 collapses in the throat between blade 1 and blade 2. On the other hand, the flow rates in each throat are affected by various factors, which not only includes the changes of pressure accompanied by the breaking off of the sheet cavity, but also the changes of local angle of attack, accompanied by rotating stall or choking.

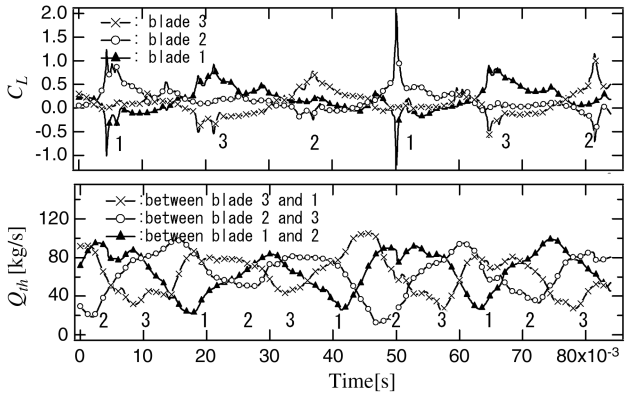

a) Super-S R.C

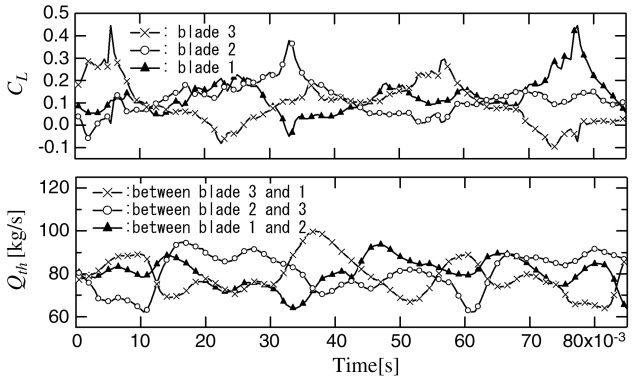

b) Sub-S R.C

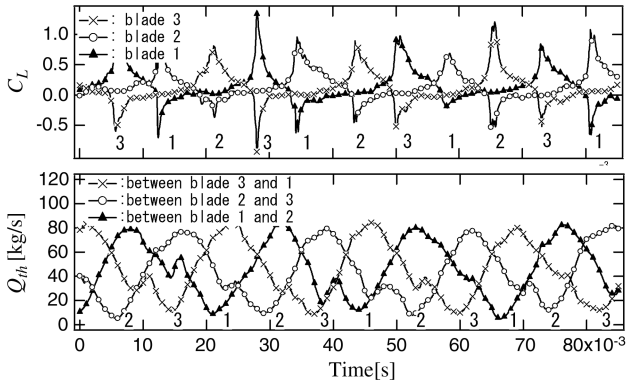

c) R-Stall C

Fig. 7 Variation of cavity volumes and throat mass flow in rotating cavitations and rotating-stall cavitation.

In sub-S RC (Fig. 7b) and R-stall C (Fig. 7c), the lifts change in the same order of blade 1–blade 2–blade 3: namely, opposite the direction of the cascade rotation (PVR < 1). At the same time, the flow rate changes in a specific order that is opposite the direction of the cascade rotation in R-stall C, which is a rotating stall, while the change in flow rate exhibits no regularity in sub-S RC. Additionally, the flow rate of super-S RC shows a peculiar waveform. The lift changes in the order of blade 3–blade 2–blade 1, the direction of cascade rotation (PVR > 1). On the other hand, the flow rate changes in the order of blade 1–blade 2–blade 3 (PVR < 1); this is the same as the order of change in flow rate in the rotating stall. These opposing orders of variation between lift and flow rate in super-S RC can be considered fundamental to the clarification of the mechanism of propagation direction of rotating cavitation. The most important point to note is that the cycle of variation of flow rate in super-S RC is half that of lift in super-S RC and almost the same as that of flow rate in R-stall C. For super-S RC, opposing orders of variation between lift and flow rate were detected in about half of the cases in this study, specifically in the cases with higher angles of attack (i.e., greater than 7°). Moreover, the variation of flow rate in the opposite direction of cascade rotation was also detected in the supercavitation condition with a lower σ, although the amplitude was very low.

D. Break-Off Frequency of Sheet Cavitation

The break-off frequency of sheet cavitations on each blade is estimated in the cases where cavitation instabilities occur. These results are shown in Fig. 8. The frequencies are averaged from several break-off cycles and the frequencies of each of the three blades. From the averaged frequencies, characteristics of the fluctuation of each cavity can be analyzed for all cavitation instabilities regardless of the propagation direction of the uneven cavity area. The break-off frequency of sheet cavities in each rotating phenomenon are, from highest to lowest, R-stall C (47-42 Hz), super-S RC (30-11 Hz), sub-S RC (19 Hz), and sync RC (0 Hz). The value of the break-off frequency in each rotating phenomenon can also be considered fundamental to the propagation direction mechanism of rotating cavitation. These values will be used later in consideration of the mechanism. Generally, in a single hydrofoil, the Strouhal number of break-off based on cavity length remains constant with decreasing cavitation number σ [29]. This means that the break-off frequency decreases with the development of sheet cavities according to a decrease in σ. Yet, in the present results, the break-off frequency in R-stall C increases to about twice that in super-S RC and sub-S RC despite occurring at a lower σ. Furthermore, this frequency is on the same order as that in cavitation surge, which is system instability. This means that R-stall C occurs contrary to the original fluctuation characteristics of unsteady sheet cavitation and is affected by the natural frequency of the cascade system.

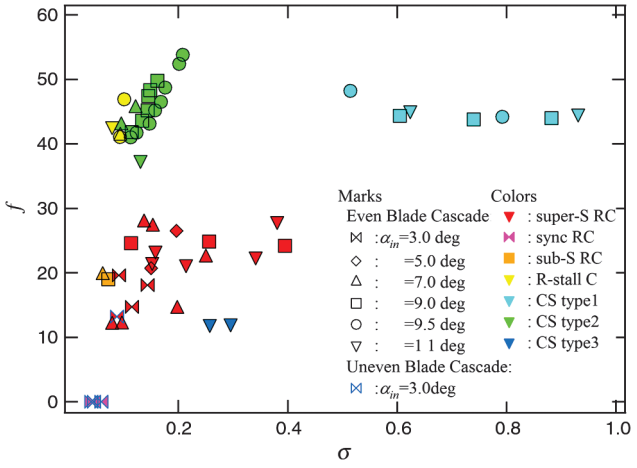

Fig. 8 Break-off frequencies of sheet cavitation in rotating cavitations and rotating-stall cavitation.

E. Consideration of the Occurrence Mechanism of Rotating Cavitations

By summarizing the results discussed thus far, the following mechanism can be proposed for the propagation direction and the appearance order of rotating cavitations and their discontinuous propagation speeds. First, it is assumed that there is a latent element of a weak rotating stall in the present cascade in spite of a gradient of the σ–ϕ curve. The existence is inferred from the throat flow rate in several cases of the present numerical results, for example, as shown in Fig. 7a. In addition, in experiments of an actual inducer, the existence of the latent rotating stall can also be inferred. A continuous peak corresponding to the rotating-stall frequency can be seen in a wide σ area, from supersynchronous rotating cavitation to sub-synchronous rotating cavitation, in the spectra of the pressure fluctuations at the inducer inlet of a three-blade [1] and four-blade [2] inducer. Next, as mentioned before, it is generally known that sheet cavities develop and their break-off frequency decreases according to the decrease in the cavitation number σ. A schematic of the change in the break-off cycle of a sheet cavity is presented in Fig. 9. Then at certain values of σ, the break-off cycle accords with the half-cycle of the latent rotating stall, the one-third cycle, the one-fourth cycle, and so forth, with a decreasing σ. Here, the rotating cavitations are considered to have been yielded at the σ. The reason underlying the occurrence of rotating cavitations at the σ is demonstrated in Fig. 10.

The waveform image of the assumed latent rotating stall is described in the first row of Fig. 10. The propagation direction of blade 1–blade 2–blade 3 is opposite the direction of cascade rotation. The frequency is assumed to be 45 Hz, which corresponds to the frequency of the rotating stalls in super-S. RC or R-stall C in the present study. The propagation velocity of the stall region is $-0.6U_t$ in the present cascade, and the propagation velocity ratio PVR is 0.4. The time interval of the transit of the stall region and the turn of the blades are described in the lower row of Fig. 10 by the blade numbers: 1 2 3 1 2 3.

1. *Supersynchronous Rotating Cavitation*

Consider a case at a certain σ, in which a sheet cavity occurs on a blade and breaks off at a frequency of 22.5 Hz. This frequency is in the range of super-S RC in the present study, as shown in Fig. 8. Then the sheet cavity breaks off once during two turns of the latent rotating-stall element. Moreover, when three sheet cavities on each blade break off asynchronously, given the circumferential symmetric property, the three sheet cavities will repeat their breaking off with even time intervals between the three cavities. At that time, if the latent rotating-stall element triggers the development of sheet cavities, the three sheet cavities will break off and develop in the order shown by the circles in the second row of Fig. 10. Consequently, the direction of apparent propagation of the uneven cavity area becomes the rotational direction of the cascade, which is blade 3–blade 2–blade 1, at this σ. If the latent rotating-stall element propagates at a regular period of 45 Hz, the break-off, with phase shifting of one-third cycle between the three cavities, will repeat

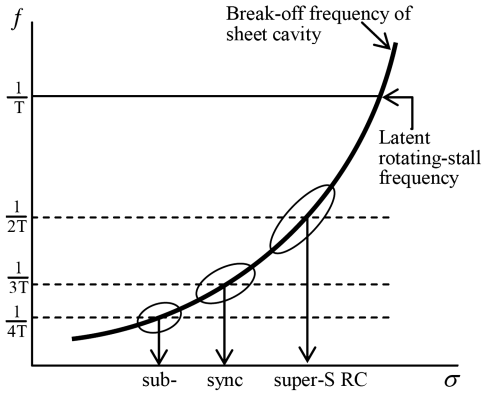

Fig. 9 Schematic of relationship between change in break-off cycle of sheet cavity and occurrence of rotating cavitations.

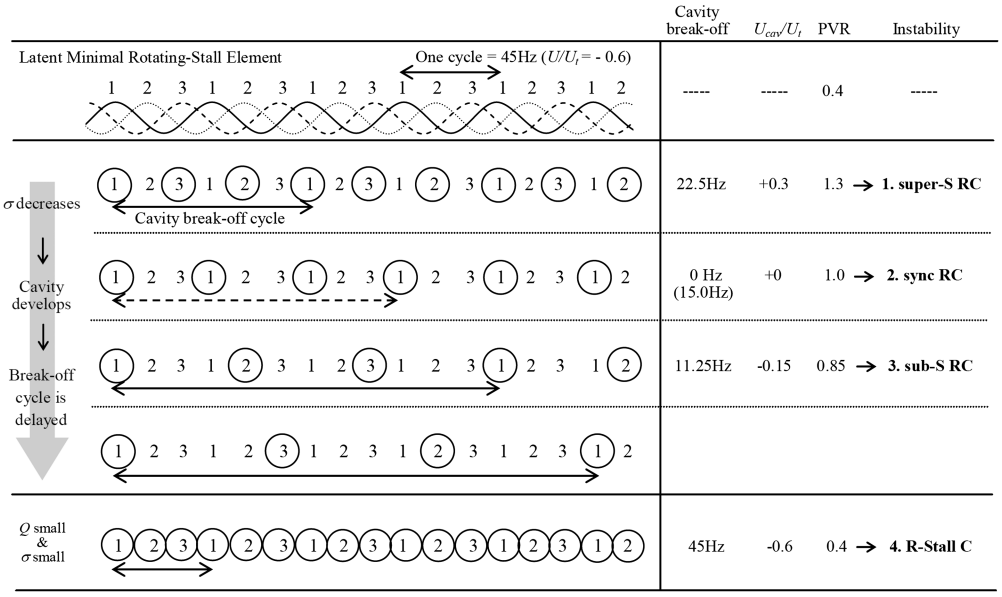

Fig. 10 Schematic of the proposed mechanism of occurrence of rotating cavitations.

stably at a break-off frequency of 22.5 Hz. This can be considered as an occurrence of supersynchronous rotating cavitation. In this case, the propagation velocity of uneven cavity area is $U_{\text{cav}} = 0.3U_t$, which is half that of the latent rotating stall, and the propagation velocity ratio becomes 1.3. This value is in the range of PVR of the super-S RC in the present study, as shown in Fig. 6, and is around the actual supersynchronous rotating cavitation in the three-blade inducer [1].

2. *Synchronous Rotating Cavitation*

When a sheet cavity develops with decreasing σ, the break-off frequency will decrease. At a certain σ lower than that of Sec. III.E.1, the sheet cavity develops to a length corresponding to a break-off frequency of 15 Hz. Then the sheet cavity will break off once during three turns of the latent rotating-stall element. This case is shown in the third row in Fig. 10. The circle in the third row that divides the break-off cycle into three parts is marked completely on blade 1. Thus means that the circumferential symmetric property cannot come into existence. Thus, the sheet cavity on blade 1 cannot break off and remains large, and variation of cavity volume accompanied by break-off cannot propagate to either the forward or backward blade. This condition is termed synchronous rotating cavitation. It is known that in an actual inducer, synchronous rotating cavitation occurs between supersynchronous and subsynchronous rotating cavitation [1,2]. In the proposed mechanism, the value of σ at which synchronous rotating cavitation occurs is lower than that at which supersynchronous rotating cavitation occurs, and the occurrence condition for synchronous rotating cavitation corresponds to the occurrence condition observed for sync RC in the present study, as can be seen in Fig. 5.

3. *Subsynchronous Rotating Cavitation*

In the case where a certain σ is lower than that in Sec. III.E.2, the sheet cavity develops to a length corresponding to a break-off frequency of 11.2 Hz at this value of σ. Then the sheet cavity breaks off once during four turns of the latent rotating-stall element. When three sheet cavities in each blade have broken off at even time intervals, for the same reason in Sec. III.E.1, break-off will occur on the blade marked by a circle in the fourth row of Fig. 10. Then the direction of apparent propagation of the uneven cavity area becomes opposite that of cascade rotation, which is blade 1–blade 2–blade 3. In this case, the propagation velocity of the uneven cavity area is $U_{\text{cav}} = -0.15U_t$, and the propagation velocity ratio is PVR = 0.85. The PVR is slightly higher than that in sub-S RC in the present study (Fig. 6) because the considered break-off frequency is lower than that in the present study. Still, the value is around the actual

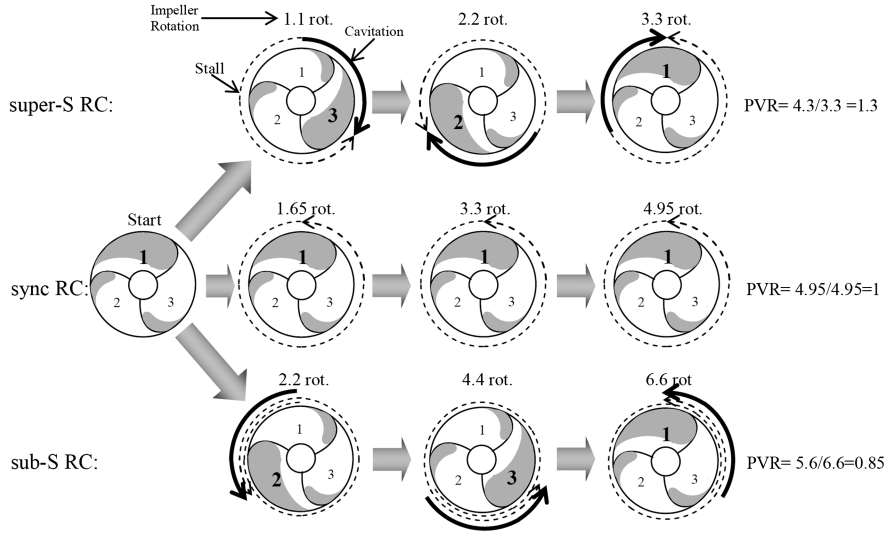

Fig. 11 Schematic diagram of the rotating cavitations in the inducer in the rotational coordinate system explained by the present mechanism.

subsynchronous rotating cavitation in the three-blade inducer [1]. In the present study, sub-S RC occurs after super-S RC, without sync RC, at the flow rate shown in the occurrence map in Fig. 5. Thus, the PVR predicted by the present mechanism is somewhat different from the PVR obtained in sub-S RC in the present study.

When σ is decreased to a value less than that in Sec. III.E.3, supersynchronous rotating cavitation recurs, as shown by the fifth row in Fig. 10. Based on the above discussion, the propagation velocity ratio will be about PVR $= 1.06$, and the break-off frequency of sheet cavity will be 9 Hz. However, at the present chord length, it is conjectured that the sheet cavity will be in super cavitation condition before it develops to the length that satisfies the frequency. In an actual inducer, supersynchronous rotating cavitation has not been observed at a σ lower than that at which subsynchronous rotating cavitation occurs. Still, the possibility exists if the inducer has a longer chord length.

4. *Rotating-Stall Cavitation*

In the case where the flow rate is at a fairly low level, the latent rotating-stall element becomes obvious and rotating stall occurs. At the same time, when σ is sufficiently low, cavitation occurs in the stall region and propagates with the rotating stall. Then the break-off frequency becomes identical to that of the rotating stall. This is the rotating-stall cavitation shown in the sixth row in Fig. 10. The occurrence mechanism is different from that of supersynchronous, synchronous, and subsynchronous rotating cavitations. The break-off frequency of a sheet cavity is the same as that of the rotating stall, which is 45 Hz, based on the assumption of a latent rotating stall. The propagation velocity ratio of the rotating-stall cavitation is 0.4. The values of break-off frequency and PVR are similar to those of R-stall C in the present study shown in Figs. 6 and 8.

Finally, a schematic diagram of the rotating cavitations in an inducer of the rotational coordinate system is shown in Fig. 11; the above-mentioned mechanism is responsible for these rotating cavitations. As shown in this figure, when the latent rotating stall triggers variations in the cavity volume, the resulting pattern of apparent propagation of cavitation corresponds to that of the rotating cavitations usually observed in inducers.

IV. Conclusions

By reproducing flowfields of several kinds of cavitation instabilities via the numerical simulation of unsteady cavitation in a three-blade cyclic cascade, it was possible to analyze in detail the unsteady characteristics of sheet cavitation in the instabilities. From the numerical results, it was shown that the well-known order of appearance of rotating cavitations, their opposite direction of propagation, and their discontinuous propagation speeds can be explained by using a unified mechanism based on the natural characteristics of a decrease in the break-off frequency of sheet cavitation and an assumption of the existence of a latent rotating stall. The following is a summary of the discussion in this study.

When the break-off cycle of a sheet cavity on a blade in a cascade is equal to the integral multiple of the latent rotating-stall cycle, rotating cavitation can be considered to occur in a stable manner. Therefore, the discontinuity of the propagation speed arises during the transition from one type of rotating cavitation to another.

The direction of the apparent propagation of rotating cavitations (supersynchronous, synchronous, or subsynchronous) is determined by the break-off cycle of the sheet cavity on a blade at a certain cavitation number. This means that because the break-off occurs with a one-third-cycle time interval between each of the three blades by the circumferential symmetric property, the uneven cavity area is seen to propagate to the forward or backward blade where the latent rotating stall is passing at the one-third-cycle timing. Thus, rotating cavitation can be regarded as occurring in the well-known order of supersynchronous rotating cavitation, synchronous rotating cavitation, and subsynchronous rotating cavitation, according to a decrease in the cavitation number.

Finally, the differences between subsynchronous rotating cavitation and rotating-stall cavitation, which have the same propagation direction but different propagation velocity, were explained from the viewpoint of differences in their occurrence mechanisms.

References

[1] Tsujimoto, Y., Yoshida, Y., Maekawa, Y., Watanabe, S., and Hashimoto, T., "Observations of Oscillating Cavitation of an Inducer," *Journal of Fluids Engineering*, Vol. 119, 1997, pp. 775–781. doi:10.1115/1.2819497

[2] Goirand, B., Collongeat, L., Dutertre, A., and Morel, P., "Vinci Fuel Turbopump Testing Activity Achievements," *Proceedings of the 4th International Conference on Launcher Technology*, 2002.

[3] Pouffary, B., Patella, R. F., Reboud, J-L., and Lambert, P-A., "Numerical Analysis of Cavitation Instabilities in Inducer Blade Cascade," *Journal of Fluids Engineering*, Vol. 130, 2008, Paper 041302. doi:10.1115/1.2903823

[4] Deshpande, M., Feng, J., and Merkle, C. L., "Nonlinear Euler Analysis of 2-D Cavity Flow," *Cavitation and Multiphase Flow Forum*, ASME Fluids Eng. Div., Vol. 135, 1992, pp. 213–219.

[5] Kubota, A., Kato, H., and Yamaguchi, H., "A New Modeling of Cavitating Flows: A Numerical Study of Unsteady Cavitation on a Hydrofoil Section," *Journal of Fluid Mechanics*, Vol. 240, 1992, pp. 59–96. doi:10.1017/S002211209200003X

[6] Delannoy, Y., and Kueny, J. L., "Two Phase Flow Approach in Unsteady Cavitation Modeling," *Proceedings of the Cavitation and Multiphase Flow Forum*, ASME Fluids Eng. Div., Vol. 98, 1990, pp. 153–158.

[7] Chen, Y., and Heister, S. D., "Two-Phase Modeling of Cavitated Flows," *Computers and Fluids*, Vol. 24, No. 7, 1995, pp. 799–809. doi:10.1016/0045-7930(95)00017-7

[8] Kunz, R. F., Lindau, J. W., Gibeling, H. J., Mulherin, J. M., Bieryla, D. J., and Reese, E. A., "Unsteady, Three-Dimensional Multiphase CFD Analysis of Maneuvering High Speed Supercavitating Vehicles," Proceedings of the 41st Aerospace Sciences Meeting & Exhibit, AIAA Paper 2003-0841, 2003.

[9] Kunz, R. F., Boger, D. A., Stinebring, D. R., Chyczewski, T. S., Lindau, J. W., Gibeling, H. J., Venkateswaran, S., and Govindan, T. R., "A Preconditioned Navier–Stokes Method for Two-Phase Flows with Application to Cavitation Prediction," *Computers and Fluids*, Vol. 29, 2000, pp. 849–875. doi:10.1016/S0045-7930(99)00039-0

[10] Shingla, A. K., Athavale, M. M., Li, H., and Jiang, Y., "Mathematical Basis and Validation of the Full Cavitation Model," *Journal of Fluids Engineering*, Vol. 124, 2002, pp. 617–624. doi:10.1115/1.1486223

[11] Singhal, A. K., Vaidya, N., and Lconard, A. D., "Multi-Dimensional Simulation of Cavitating Flows Using a PDF Model for Phase Change," ASME Fluids Eng. Div., Paper 97-3272, 1997.

[12] Hosangadi, A., and Ahuja, V., "Numerical Study of Cavitation in Cryogenic Fluids," *Journal of Fluids Engineering*, Vol. 127, 2005, pp. 267–281. doi:10.1115/1.1883238

[13] Iga, Y., Nohmi, M., Goto, A., Shin, B. R., and Ikohagi, T., "Numerical Analysis of 2-D Unsteady Cavitating Flow Around Hydrofoils in Cascade," *Transactions of the Japan Society of Mechanical Engineers. Series B*, Vol. 68, No. 666, 2002, pp. 368–374 (in Japanese).

[14] Iga, Y., Nohmi, M., Goto, A., Shin, B. R., and Ikohagi, T., "Numerical Study of Sheet Cavitation Break-Off Phenomenon on a Cascade Hydrofoil," *Journal of Fluids Engineering*, Vol. 125, No. 4, 2003, pp. 643–651. doi:10.1115/1.1596239

[15] Iga, Y., Nohmi, M., Goto, A., and Ikohagi, T., "Numerical Analysis of Cavitation Instabilities Arising in the Three-Blade Cascade," *Journal of Fluids Engineering*, Vol. 126, No. 3, 2004, pp. 419–429. doi:10.1115/1.1760539

[16] Iga, Y., Hiranuma, Y., Yoshida, T., and Ikohagi, T., "Numerical Analysis of Cavitation Instabilities and the Suppression in Cascade," *Journal of Environment and Engineering*, Vol. 3, No. 2, 2008, pp. 240–249. doi:10.1299/jee.3.240

[17] Iga, Y., Hashizume, K., Yoshida, T., and Ikohagi, T., "Occurrence Mechanism and Oscillation Characteristics of Pulsation Phenomenon Arising in Cavitation Surge in Cascade," *Journal of Environment and Engineering*, Vol. 4, No. 3, 2009, pp. 524–538. doi:10.1299/jee.4.524

[18] Ochiai, N., Iga, Y., Nohmi, M., and Ikohagi, T., "Numerical Prediction

of Cavitation Erosion Intensity in Cavitating Flows Around a Clark Y 11.7% Hydrofoil," *Journal of Fluid Science and Technology*, Vol. 5, No. 3, 2010, pp. 416–431.
doi:10.1299/jfst.5.416

[19] Yee, H. C., "Upwind and Symmetric Shock-Capturing Schemes," NASA TM 89464, 1987.

[20] Kawanami, Y., "Estimation of Cavitation Structure on a Hydrofoil and Impulsive Pressure of the Bubble Collapse," Ph.D. Thesis, University of Tokyo, Tokyo, 1999 (in Japanese).

[21] Delgosha, O. C., Patella, R. F., and Reboud, J. L., "Evaluation of the Turbulence Model Influence on the Numerical Simulations of Unsteady Cavitation," *Journal of Fluids Engineering*, Vol. 125, 2003, pp. 38–45.
doi:10.1115/1.1524584

[22] Giorgi, M. G. D., Ficarella, A., and Laforgia, D., "Comparison of Different Physical Models for the Simulation of Cavitating Flow Around a Hydrofoil," ASME Fluids Eng. Div. Paper 2005-77142, 2005.

[23] Zhou, L., and Wang, Z., "Numerical Simulation of Cavitation Around a Hydrofoil and Evaluation of a RNG *k-w* Model," *Journal of Fluids Engineering*, Vol. 130, 2008, Paper 011302.
doi:10.1115/1.2816009

[24] Li, D-Q., Grekula, M., and Lindell, P., "A Modified SST *k-ω* Turbulence Model to Predict the Steady and Unsteady Sheet Cavitation on 2D and 3D Hydrofoils," 7th International Symposium on Cavitation (CAV2009), Paper 107, 2009.

[25] Seo, J. H., and Lele, S. K., "Numerical Investigation of Cloud Cavitation and Cavitation Noise on a Hydrofoil Section," 7th International Symposium on Cavitation (CAV2009), Paper 62, 2009.

[26] Watanabe, S., Tsujimoto, Y., Franc, J-P., and Michel, J-M., "Linear Analysis of Cavitation Instabilities," *3rd International Symposium on Cavitation (CAV1998)*, 1998, pp. 347–352.

[27] Shimura, T., Yoshida, M., Kamijo, K., Uchiumi, M., and Yasutomi, Y., "A Rotating Stall Type Phenomenon Caused by Cavitation in LE-7A LH2 Turbopump," *JSME International Journal, Series B (Fluids and Thermal Engineering)*, Vol. 45, No. 1, 2002, pp. 41–46.
doi:10.1299/jsmeb.45.41

[28] Cervone, A., Bramanti, C., and Rapposelli, E., "Experimental Characterization of Cavitation Instabilities in a Two-Bladed Axial Inducer," *Journal of Propulsion and Power*, Vol. 22, No. 6, 2006, 1389–1395.
doi:10.2514/1.19637

[29] Pham, T. M., Larrarte, F., and Fruman, D. H., "Investigation of Unsteady Sheet Cavitation and Cloud Cavitation Mechanisms," *Journal of Fluids Engineering*, Vol. 121, 1999, pp. 289–296.
doi:10.1115/1.2822206

J. Oefelein
Associate Editor